Experimental study of neutrino absorption on carbon

D. A. Krakauer and R. L. Talaga
Argonne National Laboratory, Argonne, Illinois 60439

R. C. Allen,[a] H. H. Chen,[b] R. Hausammann,[c] W. P. Lee,[d] H. J. Mahler,[e] X. Q. Lu,[f] and K. C. Wang[g]
University of California, Irvine, California 92717

T. J. Bowles, R. L. Burman, R. D. Carlini,[h] D. R. F. Cochran, P. J. Doe, J. S. Frank,[i]
E. Piasetzky,[j] M. E. Potter, and V. D. Sandberg
Los Alamos National Laboratory, Los Alamos, New Mexico 87545
(Received 20 November 1991)

The process of electron emission from ~30 MeV neutrino absorption on carbon, $^{12}C(\nu_e,e^-)^{12}N$, has been observed. The flux-weighted total cross section for the exclusive neutrino-induced nuclear transition $^{12}C(\nu_e,e^-)^{12}N$(g.s.) is $[1.05\pm0.10(\text{stat})\pm0.10(\text{syst})]\times10^{-41}$ cm^2. The measured cross section and angular distribution $d\sigma/d\Omega$ are in agreement with theoretical estimates. The inclusive ν_e ^{12}C reaction rate, which accounted for the majority of all neutrino interactions observed in this experiment, was determined from a detailed fit of energy and angular distributions for the observed electrons. The inclusive $^{12}C(\nu_e,e^-)X$ cross section is measured to be $[1.41\pm0.23(\text{tot})]\times10^{-41}$ cm^2. An upper limit for the sum of the $^{13}C(\nu_e,e^-)X+^{27}Al(\nu_e,e^-)X$ inclusive absorption cross sections is presented.

PACS number(s): 25.30.−c, 13.15.Dk

I. INTRODUCTION

Low-energy neutrino-nuclear reactions present challenges and opportunities for investigations at the intersections of particle, nuclear, and astrophysics. Despite this interest in neutrino-nuclear reactions, the exceedingly small cross sections have limited the availability of experimental results. Until recently, the only exception for explicit nuclear final states was a preliminary observation [1] of the exclusive reaction $^{12}C(\nu_\mu,\mu^-)^{12}N$(g.s.) with ~150 MeV muon neutrinos. Measurements of absolute cross sections to unbound nuclear final states have been limited to deuteron breakup reactions; a measurement [2] of ^2H (ν_e,e^-) $^1H^1H$ with muon-decay neutrinos, and of the ratio of ^2H $(\bar{\nu}_e,e^+)nn$ to ^2H $(\bar{\nu}_e,\bar{\nu}_e)$ ^1H n reactions [3] for reactor antineutrinos have been reported. Given the lack of experimental results for neutrino-nucleus interactions to well-defined two-body final states, estimates and calculations of neutrino-nuclear cross sections, for example, for solar neutrinos [4], have had to be made in the absence of direct neutrino calibrations.

This report describes the measurement of two-body neutrino-nuclear reactions at energies ($E_\nu\approx20$–50 MeV) relevant to cosmic neutrino observatories and to particle and nuclear physics investigations. The exclusive reaction between specific nuclear states, $^{12}C(\nu_e,e^-)^{12}N$(g.s.), was measured by observation of the prompt electron in delayed coincidence with the subsequent ^{12}N(g.s.) decay positron; an initial report has been published [5]. Observation of the complete roundtrip from carbon to nitrogen and back to carbon represents the first "real-time" detection of neutrino-induced radioactivity and the first measurement of a neutrino-induced transition between specific nuclear states. Thus, in addition to its intrinsic scientific interest, this measurement represents a proof-of-principle demonstration of the feasibility of a new class of experiments in weak nuclear interactions.[1]

The data presented also provides absolute measurements of inclusive neutrino-nuclear absorption cross sections. Investigation of inclusive neutrino-carbon reactions was performed using detailed measurements of the angular and energy distributions of the prompt ("recoil") electrons. The total inclusive $^{12}C(\nu_e,e^-)X$ cross section was measured with 15% precision, which provides an experimental calibration point that enables the first, albeit limited, test of the nuclear physics approximations used

[a]Now at Hewlett-Packard, Palo Alto, CA 94304.
[b]Deceased.
[c]Now at Keller AG, Winterthur, Switzerland.
[d]Now at Jet Propulsion Laboratory, Pasadena, CA 91109.
[e]Now at Cerebus AG, Mannedorf, Switzerland.
[f]Now at Harvard Medical School, Boston, MA 02115.
[g]Now at Rockwell International, Thousand Oaks, CA 91350.
[h]Now at Continuous Electron Beam Accelerator Facility, Newport News, VA 23606.
[i]Now at Brookhaven National Laboratory, Upton, NY 11973.
[j]Permanent address: Tel-Aviv University, Ramat Aviv, Israel 69978.

[1]In fact, this same reaction and the related neutral current excitation of carbon, $^{12}C(\nu,\nu')^{12}C(15.1)$, have recently been measured by an experiment operating at the Rutherford ISIS beam stop [6].

to calculate neutrino-nuclear inverse-beta-decay cross sections. An attempt was made to identify inclusive neutrino reactions on other nuclei present in the detector. Although only upper limits could be derived from the data, the results indicate the feasibility of direct measurements on a variety of nuclei in the next generation of experiments.

II. CALCULATION OF RELEVANT NEUTRINO-NUCLEAR CROSS SECTIONS

There are a few published estimates for neutrino-nuclear absorption cross sections for muon-decay neutrino source spectra [7–9]. In general, the Hamiltonian for neutrino-nuclear reactions may be written in terms of the product of hadronic and leptonic current densities, $\mathcal{H} \sim \mathcal{J}_\mu^{\mathcal{H}} j_\mu^l$. Due to the pointlike nature of leptons, the matrix element for the leptonic portion is completely determined, $\langle j_\mu \rangle \sim i\bar{u}_e \gamma^\mu (1+\gamma_5) \mu_\nu$. However, evaluation of the hadronic matrix element

$$\mathcal{M} \sim \langle f \| \mathcal{H} \| i \rangle \tag{1}$$

requires a model to describe the initial ($|i\rangle$) and final ($\langle f|$) nuclear states and depends on the method used to evaluate the transition operators between these states.

Different approaches exist for calculating the nuclear transition rates. Most methods begin with the assumption [7,10] that the transition operators are one body in nature, so that the nuclear matrix elements can be expanded in terms of single-particle matrix elements in some convenient basis. Then, for electroweak semileptonic interactions, there are just seven basic classes of multipole operators [11], and only a subset of these can occur for a given transition involving initial and final nuclear states of specific angular momentum and parity. The total transition rate is proportional to the weighted sum of the transition rates between the single-particle states, where the weight factors (one-body density-matrix elements) contain the detailed connections to the nuclear many-body problem.

One approach then involves the shell model, wherein an effective Hamiltonian is solved in a limited model space to obtain the many-body wave functions, from which the density-matrix elements are calculated and the transition rate solved as the sum over one-body matrix elements known within the model. For some transitions it is possible to use experimental data from analog reactions to fit the one-body density-matrix elements as parameters, rather than calculate them microscopically [11]. Such a procedure builds in the maximum knowledge about the q^2 dependence of the individual multipole transitions that can be extracted from experiment.

Alternatives to direct shell-model calculations usually require more drastic assumptions about the q^2 dependence of the multipole matrix elements. In the elementary-particle approach [8,9,12], the momentum-transfer dependence is assumed to be universal, so that what is measured in electron scattering can be used for the neutrino analog reaction. This method is most effective when one particular multipole dominates in both instances. When two or more multipoles have significant contributions, the method may fail.

Of relevance to the present work is the reaction $^{12}\mathrm{C} \rightarrow {}^{12}\mathrm{N}$(g.s.), where the q^2 dependence of the nuclear form factors can be constrained by using existing electron scattering, muon capture, and beta-decay measurements, permitting a reasonably complete determination of the one-body density-matrix elements and hence a prediction for the neutrino cross section. Because reliable measurements are available for the associated transitions, the $^{12}\mathrm{C}(\nu_e, e^-)^{12}\mathrm{N}$(g.s.) reaction is presented as the prototypical example of this technique [7]. This is an example of a reaction where a single type of multipole dominates and where the various approaches that incorporate at least some knowledge from analog measurements all agree reasonably well. Measurement of this simple reaction provides a first experimental test of the calculational methods [7–9] in a very well-constrained case.

Transition rates between $^{12}\mathrm{C}$ and the (unbound) excited states in nitrogen are harder to estimate in that fewer data are available to constrain the one-body matrix elements and transition form factors. Consequently, there are fewer published estimates of the inclusive neutrino-absorption rate [12,7]. These transitions involve a variety of spin-isospin transfers; having neutrino cross sections for a larger set of final states (involving a variety of multipoles) may enable additional tests of the nuclear models and approximations inherent in the calculations.

It is worth noting that, in the absence of "associated" reaction data to constrain the form factors, theoretical estimates of neutrino-induced transition rates at medium energy may vary by up to 30–40 % between alternate calculational methods. When the possible "quenching" of Gamow-Teller matrix elements is considered, additional variations by as much as a factor of 3 have been reported (compare Ref. [13] to Ref. [14]). Thus, future experimental observations of some specific transitions, even with only moderate precision, would allow sensitive tests of the theoretical methodology. In particular, the very important question of Gamow-Teller quenching in neutrino-nuclear reactions could be subject to direct experimental test.

III. EXPERIMENT

A. Neutrino source

This experiment was performed at the Clinton P. Anderson Meson Physics Facility (LAMPF) where the 800 MeV proton beam provided an intense, isotropic source of electron neutrinos from stopped-muon decay in the beam stop. At typical proton currents, the beam stop was a 12 kCi source of 0–53 MeV neutrinos. The ν_e energy spectrum, displayed in Fig. 1, was completely determined by the well-known Michel distribution, $dN(E_{\nu_e})/dE_{\nu_e} \propto E_{\nu_e}^2 (X - E_{\nu_e})$, which has a maximum energy of $X = m_\mu/2 = 52.8$ MeV and peak intensity at $2/3X = 35.2$ MeV. The arrow at 17.4 MeV in Fig. 1 shows the threshold energy for the $^{12}\mathrm{C}(\nu_e, e^-)^{12}\mathrm{N}$ reaction.

The absolute flux normalization was calculated by a de-

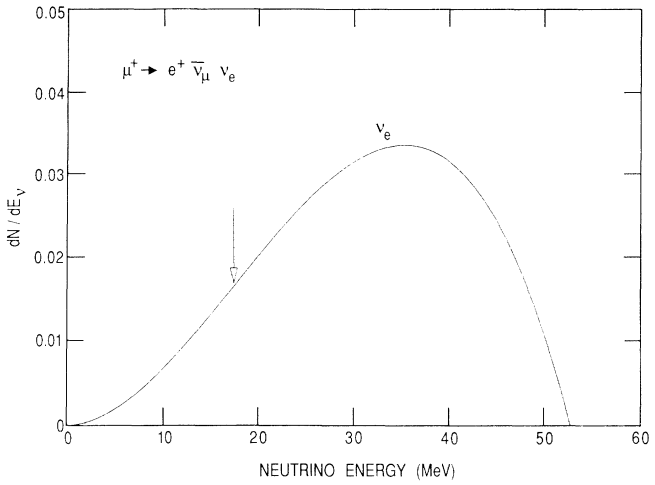

FIG. 1. Electron neutrino spectrum from $\mu^+ \rightarrow e^+ \bar{\nu}_\mu \nu_e$ at rest. The arrow indicates the threshold energy for $^{12}C(\nu_e, e^-)^{12}N$ reactions.

tailed Monte Carlo simulation of pion production, absorption, and decay in the proton beam stop [15]. The simulation was calibrated by a measurement [16] that achieved systematic normalization uncertainties smaller than 6% for stopped-pion production by protons in an instrumented simplified beam stop. Measurement of the proton current with 2% absolute precision, the scaling of the Monte Carlo to the calibration data, and the extrapolation to the actual complex beam stop configuration and geometry increased the total flux uncertainty to 7.3% [15]. For the complete beam exposure to $(1.12 \pm 0.02) \times 10^{23}$ protons, the neutrino fluence through the detector was $(9.16 \pm 0.67) \times 10^{14}$ ν_e/cm^2.

B. Apparatus and data acquisition

The neutrino detector, shown schematically in Fig. 2, was a tracking calorimeter located at a $1/r^2$-weighted mean distance of 898 cm from the neutrino source. The detector consists of 40 repeated modules of 2.5 cm thick plastic scintillation counters (2.64 g/cm^2) and 6.1 cm thick flash chamber tracking detectors (1.41 g/cm^2). This central detector was surrounded by a high-efficiency cosmic-ray veto system. In addition to measurements of the total visible energy, dE/dx, and track characteristics for the trigger ("prompt") event, the energy deposit within the central detector and hit history in the veto system were recorded during the 33 μs prior to the trigger and the 68 ms following it. The "pretrigger" information was used to discriminate against triggers due to cosmic-ray muons which interacted or stopped and decayed within the detector. The "post-trigger" data was used to identify the ^{12}N(g.s.) positron decay in delayed coincidence with the prompt electron. The visible energy measured in the scintillation counters corresponded to roughly two-thirds of the total energy deposited within the detector, with the remainder lost inside the tracking chambers. More details on the detector performance can be found in Ref. [17].

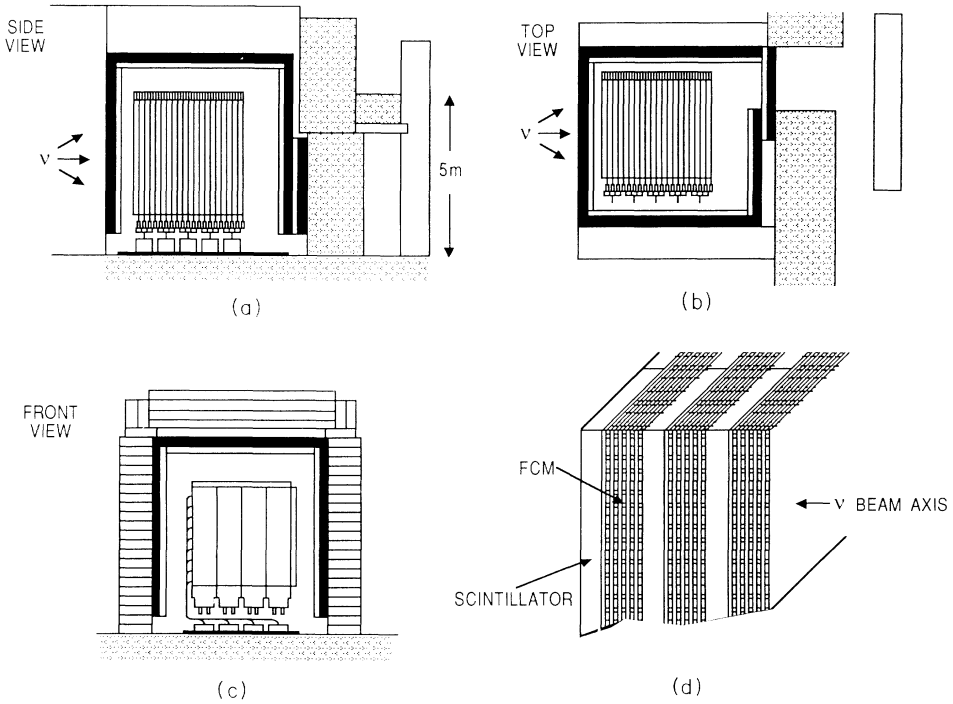

FIG. 2. Schematic diagram of the experimental apparatus showing surrounding iron (open) and concrete (shaded) shielding, active anticoincidence (dark) and segmented central detector. (a) Elevation view along beam direction, (b) plane view along beam, (c) elevation view transverse to beam, (d) exploded view of 3 of 40 layers of the central calorimeter.

TABLE I. The number of events remaining after data reduction restrictions. The final column displays the calculated detection efficiency for $^{12}C(\nu_e,e^-)^{12}N$(g.s.) events to survive all of the previous restrictions, including the energy threshold implied by the trigger requirements. Numbers preceded by × represent the fraction of events present at the previous cut level which pass the associated restrictions.

1.12×10^{23} protons $(9.16\pm0.67)\times10^{14}$ ν_e/cm^2	Beam off	Beam on	Detection efficiency ν_e ^{12}C
Triggers	562 739	223 839	0.158
Reconstructed track	‖		×0.79
Inside fiducial volume	‖		×0.88
Quiet pretrigger in veto and scint	‖		×0.95
Vis. energy and track length limits	×0.11		×0.99
No obvious backgrounds	59 088	26 892	0.114
$dE/dx \leq 1.85$ min. ioniz. particles	×0.55	×0.47	×0.98
Electron/γ sample	32 494	12 695	0.111
Hits in both views of first FCM	‖	‖	×0.97
1 or 2 scintillator "groups"	×0.67	×0.61	×0.98
Electron data set	21 773	7 752	0.106

The detector was triggered by a coincidence of three or more consecutive scintillation layers with energy deposition that was consistent with that of a single minimum-ionizing particle, and no vector signal from the anticoincidence system. Triggers collected during the LAMPF beam spill, which lasted approximately 750 μs with a repetition rate of 120 Hz, are referred to as beam-on events. The neutrino-induced event rate was only a few per day, whereas cosmic-ray interactions occurred about once per beam spill. The trigger rate, after application of the cosmic-ray veto, was roughly one trigger per 10 s of live time. About 1 in 100 triggers was caused by neutrino interactions, while almost one-third resulted from beam-associated neutron reactions and the remainder from residual (unvetoed) cosmic-ray interactions. To monitor and determine the cosmic-ray-induced event rate, additional (beam-off) triggers were collected between beam spills for roughly four times as much live time.

C. Data reduction

The data reduction was designed to retain single electrons produced in neutrino interactions, as determined by dE/dx, track and event isolation measurements. The analysis procedure [18] included several stages of restrictions, with cuts applied in parallel at each stage. Table I lists the requirements and their effect on the data sample. These restrictions are discussed in more detail in the following paragraphs. Also shown is the overall fraction of the $^{12}C(\nu_e,e^-)^{12}N$(g.s.) events retained (the integrated detection efficiency) at each stage of the analysis.

The complete data set consisted of 223 839 beam-on triggers; subtraction of the properly normalized beam-off event rate indicated that approximately 70 800 events were beam associated, primarily due to neutron interactions. The first stage of the analysis applied simple restrictions to remove obvious backgrounds. About half of all triggers, and nearly four-fifths of all beam-associated triggers, were removed from the data sample because they did not contain a reconstructed track. Events with tracks were required to be contained within the fiducial volume defined by the region between scintillation layers 2 and 39 (inclusive) and more than 5 cm from any detector edge. An additional 30% of the trigger sample was removed because the energy deposit in the scintillation counters or anticoincidence counters indicated the presence of a muon interacting or stopping within the detector during the 30 μs prior to the trigger. Finally, to uniquely define kinematic thresholds for this measurement, lower limits were placed on the event track length (three scintillation layers) and visible energy ($>$ 7 MeV); upper limits well above the kinematic range for neutrino reactions were also set. The net effect of all the above simple restrictions was to reduce the data sample by 90%; approximately 70% of triggers on neutrino interactions were retained, with the main loss due to inefficiencies of the tracking system.

A neutrino reaction produces a single electron, which appears within the detector as a single well-defined minimum ionizing track.[2] In comparison, a neutron or photon may interact several times within the detector volume, and generally will produce a hit pattern that is less consistent with being due to a single track. A simple dE/dx requirement to eliminate gamma-ray conversions and high-energy-deposit nuclear recoils caused by neutron interactions was implemented by a cut against any

[2]Bremsstrahlung radiation leads to a second cluster of measurable energy away from the main track in about 8% of all signal events.

TABLE II. Effects on the event sample of additional restrictions applied to identify ^{12}N(g.s.) decay candidates. The rightmost column displays the overall detection efficiency for $^{12}C(\nu_e,e^-)^{12}N$(g.s.) events. The final line is the result of the maximum likelihood fit to the beam-on candidates' decay-time spectrum.

	Beam-off	Beam-on	ϵ
Electron data set	21 773	7 752	0.106
Visible energy $\leq$24 MeV	‖	‖	×0.98
Contained in first 33 layers	×0.49	×0.52	×0.88
Pass all prompt cuts	10 772	4 059	0.092
Any post-trigger coincidence	×0.65	×0.68	×0.84
$4.8 \leq E_{\text{delay}} \leq 12.0$ MeV	×0.06	×0.11	×0.39
^{12}N(g.s.) decay candidates	424	304	0.030
$^{12}C(\nu_e,e^-)^{12}N$(g.s.), $^{12}N(g.s.)\rightarrow{}^{12}Ce^+\nu_e$ events		182±17	

event recording more than 4 MeV/cm (1.85 minimum ionizing particles) in any scintillation counter; 40% of all triggers were removed at the cost of a few percent of the neutrino-event sample. The third analysis stage imposed a stricter requirement on the track quality and also rejected events which contained three or more separated groups of hit scintillation counters. These two restrictions combined to reduce beam-associated backgrounds by nearly 50% while 96% of neutrino-induced events passed these restrictions.

At this stage, the data set consisted of 7752 beam-on triggers, including roughly 1400 neutrino-induced events among the 2100 beam-associated events. This so-called "electron sample" in Table I served as the base data set for the measurement of the exclusive $^{12}C(\nu_e,e^-)^{12}N$(g.s.) reaction and the inclusive $^{12}C(\nu_e,e^-)X$ reaction. However, the analysis procedures for the two measurements diverged at this stage due to the specialized requirements of the separate measurements.

IV. EXCLUSIVE $^{12}C(\nu_e,e^-)^{12}N$(g.s.) REACTION

A. Event sample

The $^{12}C(\nu_e,e^-)^{12}N$(g.s.) signal was identified by ^{12}N(g.s.) decay positrons in delayed coincidence with prompt (trigger) electrons satisfying the energetic limits for $^{12}C(\nu_e,e^-)^{12}N$ reactions. Table II lists the additional requirements applied to the data to obtain the final sample. Electrons emitted by the $^{12}C(\nu_e,e^-)^{12}N$(g.s.) reaction must have kinetic energy less than $(E_\nu^{\max}-Q)=(52.8-17.4\text{ MeV})=35.4$ MeV. Therefore, a cut was imposed to reject events with more than 24 MeV visible energy, corresponding to the kinematic limit. A second restriction reduced the fiducial volume to include only the first 33 of 40 layers of the central detector. This final cut was used because less effective cosmic-ray shielding at the back of the detector led to substantially larger backgrounds in the excluded region. The excluded region had both a high-background prompt trigger rate, and a higher-than-average rate of random post-trigger energy deposits per prompt event, as determined by the beam-off data sample.

The unique signature of ^{12}N(g.s.) decay was used to identify the $^{12}C(\nu_e,e^-)^{12}N$(g.s.) signal among the 4059 beam-on events passing all of the above kinematic restrictions on the prompt event sample. Transitions to excited states of nitrogen were not included in the delayed positron coincidence because all of these states are particle unstable. Neutrino reactions with other nuclear targets in the detector (^{13}C and ^{27}Al) produce nuclei (^{13}N and ^{27}Si) which do β^+ decay. However, the small decay energies (2.1 and 4.4 MeV, respectively) and long lifetimes (861 and 6.0 s) are distinguished from the 16.3 MeV end point, 0.016 s decay of ^{12}N.

To identify the delayed activity caused by ^{12}N(g.s.) decay, the time and pulse height of all energy deposits greater than 2.5 MeV threshold was recorded for all of the 160 scintillation counters each 16.7 μs during the 68.3 ms following every trigger. A decay positron was identified by a hit in just a single scintillator to maintain good detection efficiency.[3] The detector was not instrumented to distinguish forward and backward going tracks. Since the $^{12}C(\nu_e,e^-)^{12}N$ reaction produced electrons into both hemispheres with respect to the neutrino direction, both the first and last scintillation counters that fired during the prompt trigger were examined for delayed activity.

The search period for delayed coincidence activities in the selected scintillation counters was $0.050 \leq t \leq 66.8$ ms following the trigger. To reduce cosmic-ray backgrounds, delayed coincidences were rejected if there were signals in either the anticoincidence system during the preceding 20 μs, or in the adjacent scintillation layers during the period ±24 μs. This effectively introduced a 12.5% dead time due to the cosmic-ray rate in the veto shield and scintillators. Roughly two-thirds of all

[3]Fewer than 10% of all ^{12}N(g.s.) decay positrons caused coincidences in two scintillation counters.

prompt triggers had one or more acceptable post-trigger coincidence activities within the search region; for events with more than one delayed coincidence, only the activity with the greatest pulse height was selected for subsequent analysis.

The energy deposited by the delayed activity was determined from the observed scintillation pulse height by making a correction for the scintillation light attenuation assuming the activity was located at the same location as the prompt trigger track. Figure 3 shows the corrected energy distribution observed for delayed coincidences to the beam-off prompt events (backgrounds) in comparison with the expected spectrum of ^{12}N(g.s.) decay positrons. To separate the soft background sample from the much harder spectrum expected for decay positrons, ^{12}N(g.s.) decay candidates were required to be in the range $4.8 \leq E_{\text{delay}} \leq 12.0$ MeV. There are 304 ^{12}N(g.s.) decay candidates in the beam-on data set. The time distribution for the delayed coincidences in these events is shown in Fig. 4. The exponential enhancement due to ^{12}N(g.s.) positron decays is evident at early times after the trigger. The beam-off data, scaled by the ratio of detector live times, is shown as the histogram in Fig. 4. There is no apparent enhancement of beam-off delayed-coincidence rate at any time relative to the trigger event.

The number of events due to nitrogen beta decay was determined by a maximum likelihood fit to the delayed-coincidence time spectrum assuming an exponential decay component with a fixed lifetime of $\tau \equiv 15.87$ ms and a flat background contribution. The best fit is shown as a solid line in Fig. 4; the result is a ^{12}N(g.s.) decay signal of 181.5 ± 17.1 events on top of a background of 122.5 uniformly distributed background events. Other procedures, including binned least-squares methods and fits with unconstrained exponential lifetimes, were all found to yield signals consistent with the maximum likelihood fit, although with larger statistical uncertainties.

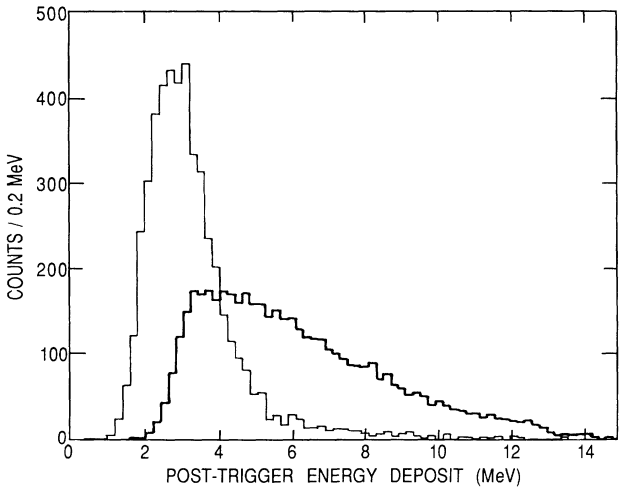

FIG. 3. Delayed coincidence energy spectra. The light histogram is the background spectrum measured in beam-off events. The heavy histogram is the Monte Carlo expectation for the ^{12}N(g.s.) decay signal.

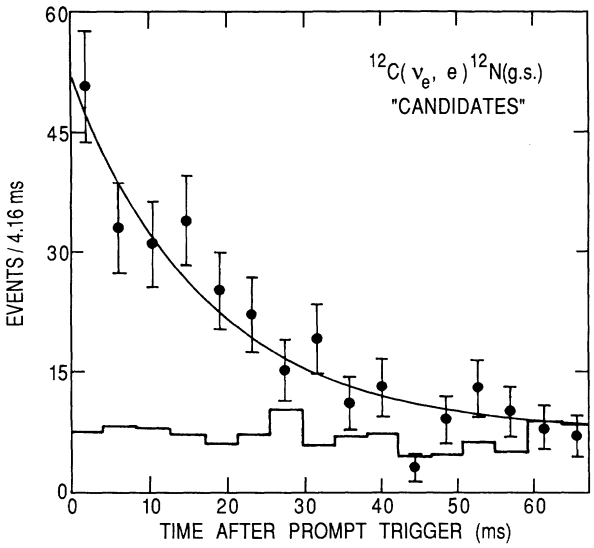

FIG. 4. Time of delayed-coincidence relative to prompt trigger. The points with errors are the beam-on candidates. The histogram is the beam-off data, scaled by relative live time. The best fit to the beam-on data is shown as a line.

B. Checks against analysis biases and exponential backgrounds

Direct tests [18] established that the background distribution was uniform in time. Possible hardware and software biases were investigated by applying the post-trigger coincidence analysis to data sets that were not expected to contain any signal. As an example, a fit to the 424 beam-off candidates shown in Fig. 4 results in an estimated decay signal of 17 ± 21 events, consistent with a completely uniformly distributed event rate. Note that this analysis of the beam-off data is identical in all respects to the beam-on event sample, except for the beam condition associated with the prompt trigger electron. To test for biases in the post-trigger coincidence selection procedure, the 4059 beam-on and 10 772 beam-off events passing all of the above prompt event restrictions were examined for delayed coincidences in random scintillation counters separated from the prompt trigger by at least three detector layers. The coincidence time spectra found by this random "mis-tagging" technique yielded an exponential signal of 6 ± 18 (12 ± 25) events in the beam-on (beam-off) sample. These tests, and all other similar explorations, indicated that the observed exponential enhancement in the final event sample was not due to hardware or software biases in the trigger, analysis, or fitting procedures.

The decay time and energy of the ^{12}N(g.s.) signal is distinct from all potential nuclear-decay backgrounds, except the possible production and decay of ^{12}B(g.s.) which has a 29.3 ms lifetime and 13.7 MeV end-point energy. Although ^{12}B beta decay cannot be statistically distinguished from the ^{12}N(g.s.) signal, a separate series of direct tests and simple calculations rule out any significant contribution to the exponential decay signal from cosmic-ray, (anti)neutrino, or neutron interactions.

A background due to cosmic-ray production of ^{12}B through neutron reactions or the muon-capture reaction $^{12}C(\mu^-,\nu_\mu)^{12}B$(g.s.) was directly ruled out by investigation of the beam-off data sample. An upper limit to the ^{12}B-induced delayed-coincidence rate, obtained from a fit to the time spectra of the 424 beam-off candidates, would have reduced the measured ^{12}N(g.s.) decay signal by less than 2.5% compared to the result obtained with a completely uniform background.

Beam-associated production of ^{12}B is possible via (n,p) and $(\bar{\nu}_e,e^+)$ reactions on carbon. The electron-antineutrino flux from the beam stop source is known experimentally [19] to be negligible, and so could not have produced measurable backgrounds via the $^{12}C(\bar{\nu}_e,e^+)^{12}B$ reaction. A direct search was unable to identify the ^{12}B(g.s.)-decay signal in different data sets enriched in neutron-induced prompt events. The 4059 beam-on events in the prompt data set of Table II include approximately 200 due to the sum of all beam-associated neutron interactions; calculations [20] suggest that the vast majority of these were due to photons produced in neutron bremsstrahlung and radiative capture with a conservative worst-case upper limit of fewer than five (n,p) events in the final ^{12}N(g.s.) sample. Since there was no evidence for the presence of any exponential background and the limits to the beam-associated backgrounds were quite small, the statistical uncertainty of ± 17 events is taken to also account for any systematic biases introduced by backgrounds.

C. Measurement of the exclusive cross section

The exclusive cross section, $\sigma(^{12}C(\nu_e,e^-)^{12}N(g.s.))$ can be extracted from the observed number of events, $N=181.5\pm17.1$, according to $\langle\sigma\rangle=N/\epsilon\phi T$, where ϵ is the flux-weighted integrated detection efficiency, ϕ is the integrated neutrino flux, and T is the number of target nuclei. Table III lists the experimental values and uncertainty associated with these quantities. The detector (which was also the neutrino target) contained 12.8 metric tons of carbon, or $T=(6.36\pm0.13)\times10^{29}$ ^{12}C nuclei. The neutrino exposure has already been mentioned, $\phi=(9.16\pm0.67)\times10^{14}$ ν_e/cm^2.

The detection efficiency, ϵ, was determined by a detailed ESG4–based Monte Carlo simulation of the detector response to electrons. The entire cascade, including the prompt electron from $^{12}C(\nu_e,e^-)^{12}N$(g.s.) and the delayed positron from $^{12}N\rightarrow{}^{12}C\ e^+\nu_e$ was simulated. The differential distributions, $d^2\sigma/d\Omega\,dE_e$, for the prompt reaction were calculated according to programs provided by Donnelly [7,21]. The positron-decay spectrum included corrections for the Coulomb effect and decay branches to excited states in carbon. Simulated events that met the trigger requirements were passed through the same analysis programs as the real data. The detection efficiency is defined by the number of events generating a trigger and passing all restrictions normalized by the total number simulated.

TABLE III. Values and uncertainties of quantities used to determine the $^{12}C(\nu_e,e^-)^{12}N$(g.s.) cross section.

Experimental quantity	Central value	Uncertainty (%)
Observed event rate N	181.5	9.4(stat)
Detection efficiency ϵ	0.0297	6.4(syst)
Neutrino flux ϕ	9.16×10^{14} ν_e/cm^2	7.3(syst)
Target thickness T	6.36×10^{29} ^{12}C	2.0(syst)

The calculated efficiency for triggering on and detecting the prompt electron from $^{12}C(\nu_e,e^-)^{12}N$(g.s.) was 0.0917; the fraction of all subsequent ^{12}N(g.s.) decays detected by the post-trigger analysis was 0.324. The combined efficiency was 0.0297 ± 0.0019, where the error properly reflects the combined systematic uncertainties of the simulation, theoretical distributions, and analysis procedures. The errors associated with the tracking, energy-related restrictions, and dead times were estimated from the range of results obtained when the appropriate parameters (e.g., photoelectrons/MeV, flash chamber tube hit efficiency, etc.) were varied; the uncertainties are 4% due to tracking requirements, 3% due to the energy scale for prompt cuts, 3% for uncorrelated uncertainties in the post-trigger energy scale, 1% for pretrigger activities in the shield and scintillators, and 2.5% from the dead times in the post-trigger search period. The quadrature sum of these independent errors results in a fractional uncertainty of $\Delta\epsilon/\epsilon=6.4\%$.

Combining these experimental factors with the observation of 181.5 ± 17.1 ^{12}N(g.s.) decay events, the measured neutrino-flux-weighted exclusive cross section is

$$\langle\sigma(^{12}C(\nu_e,e^-)^{12}N(g.s.))\rangle$$
$$=[1.05\pm0.10(\text{stat})\pm0.10(\text{syst})]\times10^{-41}\ \text{cm}^2\ . \quad (2)$$

The statistical error (9.4%) includes the systematic uncertainties introduced by the fitting procedure, and the systematic errors (9.9%) include the uncertainties in the overall detection efficiency (6.4%), in the neutrino flux (7.3%), and in the target composition (2%) added in quadrature. If one assumes that the neutrino-absorption cross section above threshold Q has a $(E_\nu-Q)^2$ dependence on the neutrino energy E_ν, then the flux-weighted cross section obtained with muon-decay neutrino beams is equivalent to the cross section for monoenergetic neutrinos with $E_\nu=35$ MeV.

Two examples are given of tests [18] performed to show that the reported cross section is not systematically biased by the analysis procedure; i.e., that the Monte Carlo evaluation of detection efficiencies can properly account for changes in the analysis as a function of energy thresholds and in techniques to select post-trigger signals. First, as a test of the calculated efficiency for restrictions to the prompt sample, the delayed-coincidence analysis was applied to the complete data set of 7752 beam-on and 21 773 beam-off events in the "electron data set" of Table I. 645 beam-on and 1366 beam-off candidates were selected, and the ^{13}N(g.s.) decay signal in the beam-on data was 218.7 ± 23.7. The additional cuts to the prompt event sample (listed in Table II), which increase the signal-to-noise ratio by a factor of 3, are expected to reduce the ^{12}N(g.s.) signal by a factor of 0.86. There is

good agreement between the expected reduction with the measured ratio of 0.83 ± 0.10 between the final data set and the set without additional restrictions to the prompt event sample.

To test the post-trigger analysis, the observed ^{12}N(g.s.)-decay signal was investigated as a function of the lower threshold L applied to the post-trigger energy, $L \leq E_{\text{delay}} \leq 12$ MeV. Figure 5 shows the number of candidates found, and the nitrogen-decay signal determined from the time spectra, for various values of the threshold. The plot clearly shows the general improvement in signal-to-noise ratio (or ratio of signal events to total candidates) as the threshold was raised. Consistent values of the cross section were obtained independent of the post-trigger energy threshold even as the measured signal (and detection efficiency) varied by more than a factor of 2.

As a further confirmation of the agreement between the simulation of the signal and the observed data, the kinematic distributions calculated for prompt electrons from ^{12}C(ν_e,e^-)^{12}N(g.s.) are compared to the observed distributions for prompt electrons selected by their post-trigger characteristics. This comparison is made for an enriched ($S/N \sim 4/1$) sample of signal events obtained by exploiting the rapid decline in background activity relative to the beta-decay signal for higher post-trigger energy thresholds (see Fig. 5). 161 candidates were selected by requiring $5.5 \leq E_{\text{delay}} \leq 12.0$ MeV; the signal estimated by the likelihood fit is 128 ± 14 events. Figure 6 shows the kinematic distributions of visible energy, reconstructed $\cos\theta_{e\nu}$, and absolute value of $\cos\theta_{e\nu}$ for data and Monte Carlo simulation. A similar comparison using a partially independent sample has been presented previously [5]. The good agreement shown in Fig. 6 suggests that the simulation accurately predicts the detector response to the signal reaction.

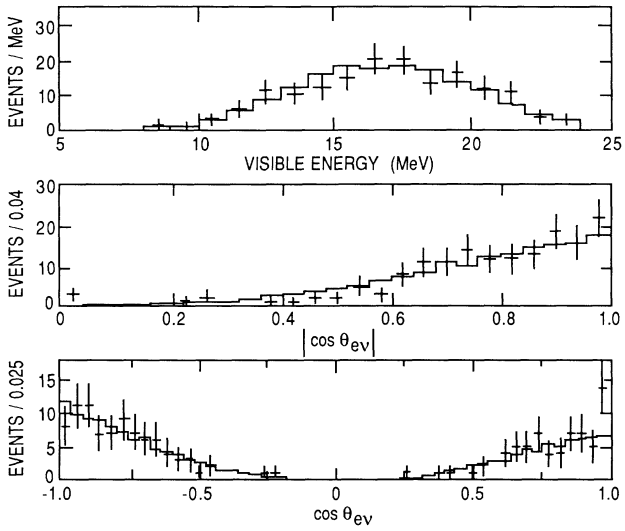

FIG. 6. Observed kinematic distributions of prompt events selected because of high delayed energy deposit. The data (and statistical errors) are shown by the vertical crosses. The histogram is the Monte Carlo simulation of ^{12}C(ν_e,e^-)^{12}N(g.s.) normalized to the data. (Top) Visible energy. (Middle) Cosine of angle between incident neutrino and measured electron track. (Bottom) Same as above, except the delayed coincidence location has been used to determine the absolute direction of the electron.

V. INCLUSIVE ^{12}C(ν_e,e^-) REACTION

A. Event sample

Inclusive ν_e ^{12}C reactions to ^{12}N excited states do not have a delayed-time signature. In contrast to the exclusive reaction to the ^{12}N(g.s.), which was identified by coincidence activity, the inclusive events were identified solely by the kinematic distributions of the prompt electrons and their differences relative to the background processes. Therefore, it was critical that the data set contain only well-measured electrons; the presence of events beyond the kinematic limits of the ν_e ^{12}C signal was used to pin down the contribution of backgrounds.

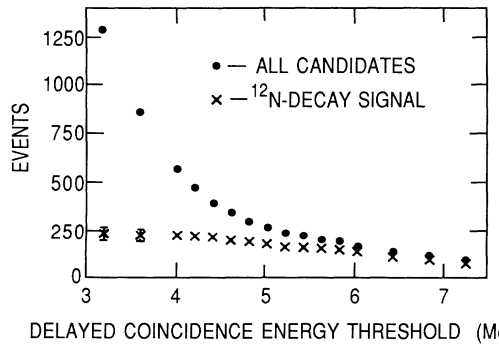

FIG. 5. Number of post-trigger coincidences (candidates) and fitted ^{12}N(g.s.) decay signal vs delayed energy threshold.

Several additional cuts were applied to the electron data set of Table I in order of reduce neutron and cosmic-ray backgrounds to the ν_e ^{12}C signal. The resulting data set has been previously reported [19,22]; it was primarily intended to measure νe^- elastic scattering [22], but the inclusive ^{12}C(ν_e,e^-)X cross section may be extracted simultaneously. Unlike the exclusive event sample (Table II), for this measurement the fiducial volume included all of layers 2-39 and no total-energy restrictions were applied. Table IV lists the three different restrictions that were applied to remove ambiguous events likely to be caused by backgrounds. (1) Events were eliminated if any scintillator along the primary track recorded $dE/dx < 1.2$ MeV/cm. This removed fewer than 2% of the ν_e ^{12}C signal but roughly 10% of the cosmic-ray backgrounds. (2) Events with two separate groups of hit scintillators were eliminated if the downstream group contained three or more counters. About 6% of ν_e ^{12}C events were removed, which corresponded to the fraction of events with radiated photons detected away from the downstream primary electron track. (3) A statistic combining the dE/dx, the distance of closest approach of the track to a detector edge, and the reduced χ^2 of the track fit was used as a likelihood parameter to identify events correlated with the tails of distributions known to be use-

TABLE IV. Additional restrictions applied to achieve the final event sample. The last column is the detection efficiency for inclusive $^{12}C(\nu_e,e^-)X$ reactions. The bottom line is the result from the maximum likelihood fit to the $(E_{vis},\cos\theta_{ev})$ distributions.

	Beam-off	Beam-on	ϵ
Electron data set	21 773	7 752	0.100
$dE/dx \geq 0.5$ min. ioniz. part.	‖	‖	×0.98
<3 downstream scintillators	‖	‖	×0.94
Likelihood parameter cut	×0.60	×0.63	×0.83
Neutrino event data set	12 988	4 880	0.076
Beam-associated events		1 492±76	
$^{12}C(\nu_e,e^-)X$ events		626±71	

ful in identifying backgrounds. A cut was defined which retained 83% of the ν_e ^{12}C signal and eliminated nearly half of the beam-associated (neutron) backgrounds.

The remaining data sample of 4880 beam-on events includes 1492±76 beam-associated events. Figure 7 displays the angular $\cos\theta_{e\nu}$ and visible energy E_{vis} distributions of the beam-associated data. The beam-associated events were presumed to be the sum of contributions from the neutrino-carbon inverse-beta-decay signal of interest here, and several backgrounds, namely, neutrino-electron elastic scattering, neutrino absorption by other isotopes, and neutron-induced gamma rays. The expected event rates R for each of the neutrino-induced backgrounds and for the $^{12}C(\nu_e,e^-)X$ signal have been estimated from the calculated beam-weighted cross section $\langle\sigma\rangle$, integrated target density T, estimated acceptance $\langle\epsilon\rangle$, and neutrino fluence ϕ, according to $R=\langle\epsilon\rangle\phi T\langle\sigma\rangle$. These quantities are listed in Table V.

B. Determination of the $^{12}C(\nu_e,e^-)X$ signal

The $^{12}C(\nu_e,e^-)X$ signal was extracted from the data, and the backgrounds were determined empirically by a multiparameter maximum likelihood fit to the visible energy, observed recoil angle (E_{vis} vs $\cos\theta_{e\nu}$) distributions. The object of the fit was to determine the relative contribution from each of the contributing reactions. The data was sorted into 323 $(19E_{vis}\times 17\cos\theta_{e\nu})$ unequally sized bins. The likelihood function was calculated,

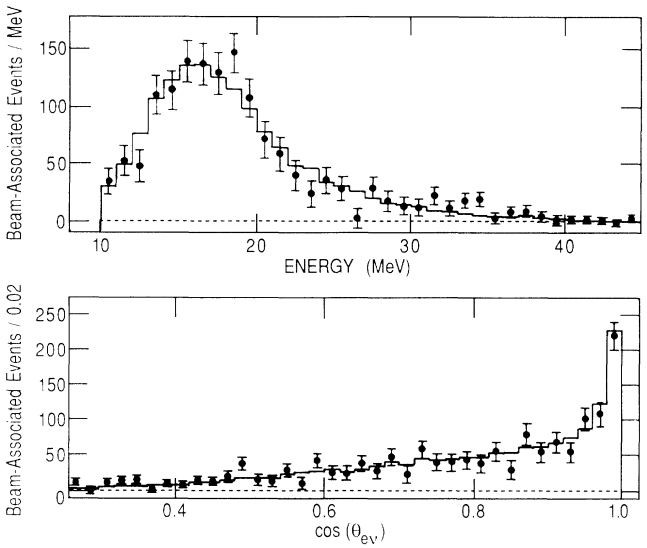

FIG. 7. Observed kinematic distributions for the beam-associated data sample. The data is shown as points with errors, the histogram is the best fit to the data. (Top) Visible energy. (Bottom) Cosine of angle between incident neutrino and measured electron track.

$$\mathcal{L}(R_k)=\sum_{i=1}^{323}[2(N_i^{fit}-N_i^{obs})-2\ln(N_i^{obs}/N_i^{fit})]\ , \qquad (3)$$

where N_i^{obs} was the observed event rate in bin i, and $N_i^{fit}=\sum_k R_k f_k(i)$ was the expected event rate in bin i assuming a total of R_k events of type k, $k=(\nu_e\ ^{12}C,\nu e^-,\nu_e(^{12}C+^{27}Al),np\gamma,CR)$ in the whole data set. R_k were the free parameters of the fit, and $f_k(i)$ were distributions described below. In order to avoid negative bin populations introduced by a subtraction of the beam-off (cosmic-ray, CR) contribution, the fit was performed on the beam-on data set, with the CR shape $f_{CR}(i)$ given by spline fits to the observed data and the normalization R_{CR} fixed to the measured value.

The distributions $f_k(i)=f_k(E_{vis},\cos\theta_{e\nu})$ of the beam-associated backgrounds, and the neutrino-carbon absorption signal, were taken from detailed Monte Carlo simulations. Neutrino nuclear reactions were generated according to double-differential distributions $d^2\sigma/d\Omega\,dE_e$ supplied by Donnelly [21] for specific nuclear transitions, and summed over all relevant transitions. Figure 8 shows the neutrino-flux-weighted distributions of electron angle

TABLE V. Sources of events in the final data sample. The fourth row represents neutron-induced gamma-ray background events. The expected rate is evaluated for $\phi=9.16\times10^{14}$ cm^{-2} electron neutrinos. The $^{12}C(\nu_e,e^-)X$ total cross-section measurement is based on the event rate determined by the best fit shown in the rightmost column.

Reaction	Targets $T(10^{29})$	$\langle\sigma\rangle$ 10^{-42} cm^2	$\langle\epsilon\rangle$ %	Expected rate	Best fit
$\nu_e\ ^{12}C$	6.36	13.2	7.6	583	626±71
$(\nu_e+\nu_\mu+\bar{\nu}_\mu)e^-$	49.5	0.4	15.7	284	295±35
$\nu_e(^{13}C+^{27}Al)$	0.17	116.1	15.6	282	136±102
$np\rightarrow\gamma$					435±90

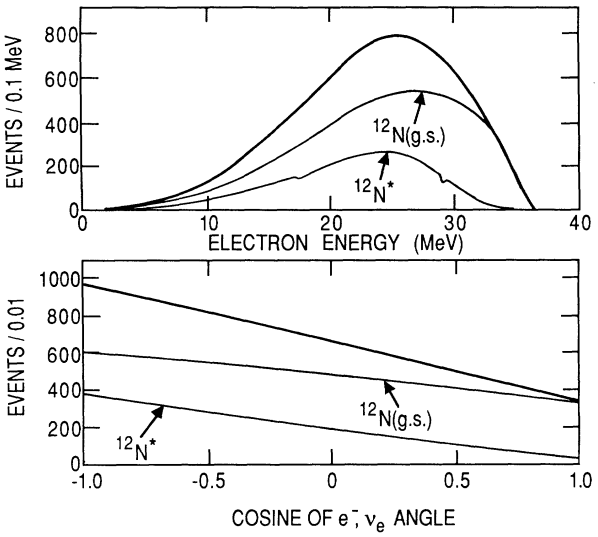

FIG. 8. Neutrino-flux-weighted distributions of electrons from neutrino absorption on carbon, as generated for input to the Monte Carlo simulation. The contributions from exclusive reactions to the nitrogen ground state, reactions to all nitrogen excited states, and the sum (all final states) are shown separately. (Top) Electron kinetic energy. (Bottom) Cosine of scattering angle between incident neutrino and outgoing electron.

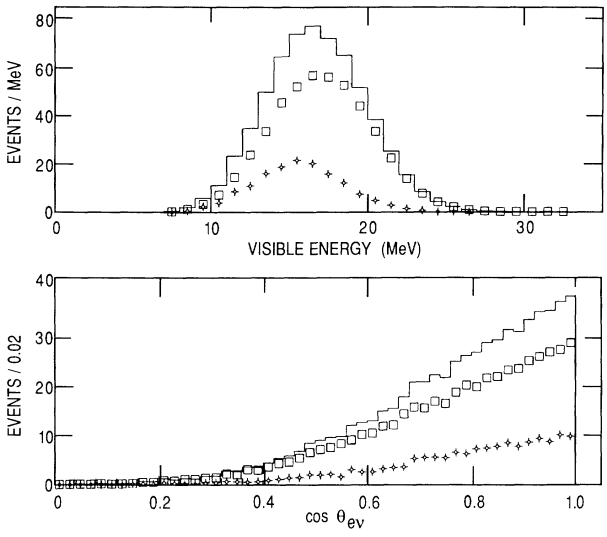

FIG. 9. Monte Carlo results for expected measured distributions for electrons produced in ν_e ^{12}C reactions. The contributions from the exclusive reaction to the nitrogen ground state (open boxes), reactions to all nitrogen excited states (circles), and the sum to all final states (histogram) are shown. (Top) Visible energy. (Bottom) Cosine of angle between incident neutrino and measured electron track.

and kinetic energy for ^{12}C(ν_e,e^-)^{12}N(g.s.) and ^{12}C(ν_e,e^-)^{12}N* (nitrogen excited state) reactions, as generated for input to the Monte Carlo simulation. Figure 9 shows the expected shape of the observed visible energy and measured (ν,e^-) angular distributions according to the Monte Carlo simulation of the detector response to the generated electron distributions. For the $f_{\nu_e{}^{12}\mathrm{C}}(i)$ distribution used in the fit, shown as the histogram in Fig. 9, the relative contributions obtained for transitions to the ^{12}N ground state and to the excited states were normalized according to the calculated cross sections [21] and efficiencies.

The input distributions for background reactions were generated in accordance with the best knowledge of the underlying processes. The neutrino-electron scattering events were generated assuming $\sin^2\theta_W = 0.23$. The neutron-induced γ rays were generated [20] according to a rapidly falling spectrum appropriate for $np\gamma$ bremsstrahlung and radiative capture on protons, plus a small contribution from giant resonance capture. The neutrino-nuclear backgrounds were the weighted sum of expectations from ν_e ^{13}C and ν_eAl reactions, including best estimates of the ground-state, allowed, and first-forbidden contributions to the cross sections [21] in each nuclei. Figure 10 shows the Monte Carlo expectations for the E_{vis} and $\cos\theta_{ev}$ distributions of the beam-associated background events in comparison to the ^{12}C(ν_e,e^-)X signal. The elastic-scattering background was distinguished by its forward-peaked angular distribution. The main distinction between inclusive ν_e ^{12}C events and the other background processes was in the visible energy.

The result of the maximum likelihood fit using these distributions is given in the final column of Table V, and is shown as the solid histogram on top of the data in Fig. 6. The measured ^{12}C(ν_e,e^-)X inclusive absorption signal is 626±71 events. The experimentally determined

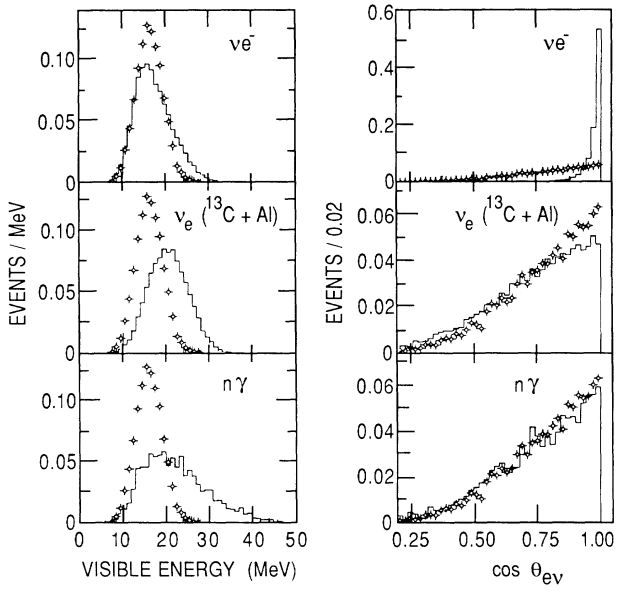

FIG. 10. Monte Carlo results for expected measured distributions for the named beam-associated backgrounds (histogram) compared to expectations for ν_e ^{12}C signal (circles). All distributions are normalized to unity. (Left) Visible energy. (Right) Cosine of angle between incident neutrino and measured electron track.

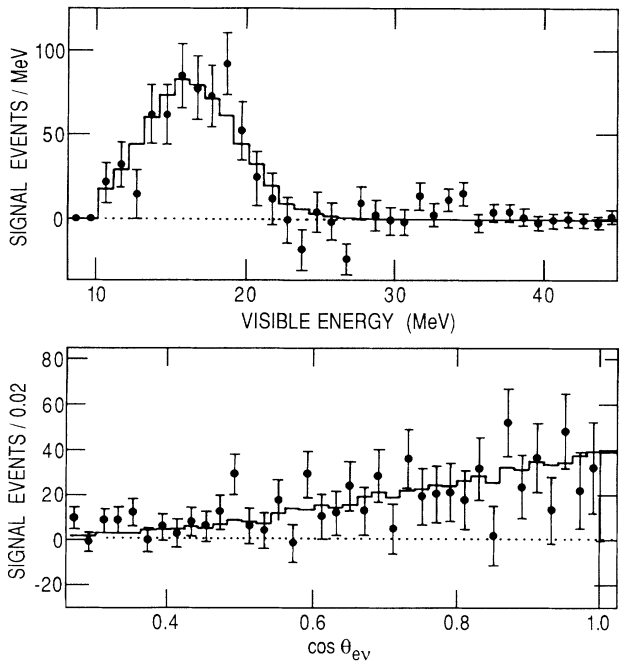

FIG. 11. Comparison of Monte Carlo expectation for $^{12}C(\nu_e,e^-)X$ signal (histogram), normalized to results to fit, compared to data (points with errors) after all cosmic-ray and beam-associated backgrounds have been subtracted. (Top) Visible energy. (Bottom) Cosine of angle between incident neutrino and measured electron track.

neutrino-induced background rates are in fair agreement with the expected rates. The neutron-induced event rate is within a factor of 2 of the results of an absolutely normalized calculation. In Fig. 11, the normalized $^{12}C(\nu_e,e^-)X$ distribution is plotted with the data remaining after all cosmic-ray and beam-associated backgrounds have been subtracted according to the results of the fit. The extracted $^{12}C(\nu_e,e^-)X$ signal is not sensitive to the detailed assumptions about the background component distributions. Several fits were attempted with alternative assumptions about the background distributions, but all gave consistent estimates of the ν_e ^{12}C signal. Table VI summarizes results of some of these tests.

C. Inclusive cross section

Proper evaluation of the $^{12}C(\nu_e,e^-)X$ cross section depends on proper evaluation of the integrated detection efficiency for the associated electrons. Transitions to the ^{12}N(g.s.) had a lower threshold, and, consequently, produced higher-energy electrons than did transitions to excited states in nitrogen. Therefore, the integrated detection efficiency for "exclusive" reactions to the nitrogen ground state, 8.1% was slightly higher than for reactions to the excited states, 6.5%; the combined efficiency was $\epsilon=7.6\pm0.4\%$ when weighted according to calculated transition strengths. The inclusive ν_e absorption cross section for ^{12}C is obtained by combining the observation of $N=626\pm71$ ν_e ^{12}C events with the other experimental parameters:

$$\langle\sigma(^{12}C(\nu_e,e^-)X)\rangle = [1.41\pm0.16(\text{stat})\pm0.19(\text{syst})]\times10^{-41}\ \text{cm}^2\ , \quad (4)$$

where the (syst) error is the quadrature sum of the uncertainties in the Monte Carlo simulation (5%), neutrino flux (7.3%), target density (2%), and an estimate of the uncertainty in overall detection efficiency ϵ introduced by ambiguities in the relative weighting of the nitrogen ground-state and various excited-state contributions to the total event rate (7%).

The ν_e ^{12}C signal rate and corresponding cross-section measurement were stable against changes in the hypothesis about the relative normalization of the contributions from transitions to the nitrogen ground state and excited states. As shown in Table VII, the maximum likelihood ν_e ^{12}C signal obtained is consistent when the relative normalization of the ground-state and excited-state contributions is varied between 0% (all excited-state transitions) to 100% (all ground-state transitions). The last column shows the results when both the excited-state and ground-state transitions are included as independent parameters of the fitting procedure; with the relative normalization of each contribution unconstrained, the fit indicates a (65%/35%) split between events to the nitrogen ground state and to nitrogen excited states. All hypotheses about the final-state distribution yield consistent values for the measured cross section.

TABLE VI. Comparison of fit results for different hypotheses about the source of background events contributing to the final event sample. A blank line indicates the source is neglected completely. The cosmic-ray contribution is fixed except when shown with ± errors.

Event type	Best fit	Fit type CR rate unconstrained	No. neutron contribution	No. ν_e abs. on $^{13}C+Al$
χ^2/d.f.	413/320	413/319	440/321	415/321
ν_e ^{12}C	626±71	600±87	660±72	671±94
νe^-	295±35	293±36	317±38	295±35
$\nu_e(^{13}C+Al)$	136±102	122±102	515±69	
$np\rightarrow\gamma$	435±90	396±115		526±62
Cosmic ray	3388	3470±162	3388	3388

TABLE VII. Comparison of fit results for different assumptions about the ν_e ^{12}C final-state distribution. The cosmic-ray contribution is fixed at 3388 events for all fits shown here. The errors are statistical only. The best fit (see Table VI) used in the analysis of the total cross section is performed with the (g.s.)/(total) event rate contribution fixed at 76%.

Event type	Ratio of (g.s.)/(excited) 0% (g.s.) 100% (excited)	25% (g.s.) 75% (excited)	50% (g.s.) 50% (excited)	100% (g.s.) 0% (excited)	Ratio unconstrained
χ^2/d.f.	411/320	415/320	413/320	413/320	410/321
ν_e ^{12}C	587±67	641±95	683±71	714±91	716±111
νe^-	298±35	293±36	292±35	297±35	292±36
ν_e(^{13}C+Al)	183±92	125±93	75±93	−15±111	−20±108
$np\rightarrow\gamma$	424±98	399±96	442±96	496±98	504±97

VI. OTHER NEUTRINO-NUCLEAR ABSORPTIONS

In principle, ν_e charged-current reactions with ^{13}C and ^{27}Al nuclei may be visible in this experiment because they produce electrons at energies above the kinematic limit for electrons from ^{12}C inverse-beta decay and at angles larger than for νe^- elastic scattering. The expected neutrino-absorption cross sections are large because of the relatively low threshold energies, and the detected event rate further enhanced by the higher overall detection efficiency associated with the greater recoil-electron energies. Although these nuclei were each only 1% as abundant as ^{12}C, the expected absorption event rate was non-negligible, as evidenced in Table V.

The best fit to the observed data set, given in Table V of the previous section, showed marginal evidence for neutrino reactions with other nuclei, 136±102 events; the effect was not stable when the parameters and hypothesis of the fit were altered. If the observed event rate is interpreted as an upper limit, then at 90% confidence level, fewer than 272 ν_e(^{13}C+Al) events were detected.

The detector contained $T=0.71\times10^{28}$ ^{13}C target nuclei and 1.08×10^{28} ^{27}Al nuclei. The Monte Carlo estimated detection efficiency for inclusive ν_e ^{13}C events was $\epsilon=0.165$; for ν_e Al the detection efficiency was 0.150. The upper limit of 272 observed events is equivalent to an upper limit on the weighted sum of the ^{13}C$(\nu_e,e^-)X$ and ^{27}Al$(\nu_e,e^-)X$ cross sections,

$$\langle\sigma(\nu_e\text{Al})\rangle+0.723\langle\sigma(\nu_e\,^{13}\text{C})\rangle < 18.3\times10^{-41}\,\text{cm}^2\ (90\%\ \text{CL})\ . \quad (5)$$

Alternatively, Eq. (5) may be regarded as an upper limit of $\langle\sigma\rangle<10.6\times10^{-41}$ cm^2 on the mean of the ν_e absorption cross sections for ^{13}C and Al.

VII. DISCUSSION AND COMPARISON OF MEASURED CROSS SECTIONS WITH THEORETICAL CALCULATIONS

A. Exclusive ^{12}C$(\nu_e,e^-)^{12}$N(g.s.) cross section

The flux-weighted cross section is measured to be $\langle\sigma\rangle=(1.05\pm0.14)\times10^{-41}$ cm^2, where the statistical and systematic errors have been added in quadrature. Donnelly has calculated the muon-decay neutrino-flux-weighted cross section to be 0.94×10^{-41} cm^2 [7,21]. Subsequent publications by other authors quote 0.90×10^{-41} cm^2 [8] and 0.92×10^{-41} cm^2 [9]. Each of the referenced calculations [7–9] makes explicit use of measured analog transition rates to constrain the form factors and matrix elements for the neutrino reaction; with such constraints the uncertainties in the theoretical estimates are expected to be less than 10%. This measurement is in good agreement with the theoretical calculations, which confirms that the complementary nuclear transition data can be used to predict the neutrino-induced reaction rate. Theoretical results [12] which did constrain form factors using results from analog reactions underestimate the present measurement by 30%.

The good agreement of the observed visible energy with expectations from the Monte Carlo simulation, as shown in Fig. 6, is consistent with the expected $(E_\nu-Q)^2$ energy dependence of the inverse-beta-decay cross section. The observed angular distributions are also in good agreement with the simulation. The differential cross section $d\sigma/d\Omega$ is parametrized by a $1+A\cos\theta$ distribution; the effect of the nuclear form factors is expected to reduce the asymmetry from the pure Gamow-Teller value ($A=-\frac{1}{3}$) to roughly $A\approx-0.3$. Experimentally, a fit to the nitrogen decay signal as a function of angle yields $A=-0.167\pm0.152$, in reasonable agreement with expectations.

B. Inclusive ^{12}C(ν_e,e^-) cross section

The measured flux-averaged inclusive neutrino-absorption cross section is $(1.41\pm0.23)\times10^{-41}$ cm^2, implying a cross section to nitrogen excited states of approximately 0.36×10^{-41} cm^2. The ratio of (exclusive)/(inclusive) cross sections [^{12}N(g.s.)final state versus all final states] is

$$\mathcal{R}=0.74\pm0.11(\text{stat})\pm0.06(\text{syst})\ . \quad (6)$$

As an alternative, but not independent, method of determining the cross section to nitrogen excited states, the likelihood fit to the kinematic distributions of the final data set (of Table IV) was repeated with a separate ^{12}N(g.s.) contribution, fixed by the measured exclusive cross section [Eq. (2)], and a ^{12}N* excited-state contribution as a free parameter of the fit. The result was 204±70

excited-state events, corresponding to an excited-state cross section of $(0.54\pm0.19)\times10^{-41}$ cm^2. The total inclusive cross section $(1.59\pm0.26)\times10^{-41}$ cm^2 and (exclusive/inclusive) ratio [$\mathcal{R}=0.66\pm0.11$(stat) ±0.02 (syst)] are consistent with the results of the primary method adopted above.

Donnelly [7,21] estimates the inclusive ν_e ^{12}C absorption cross section to be 1.31×10^{-41} cm^2, including 0.37×10^{-41} cm^2 due to transitions to nitrogen excited states. 99% of the excited-state contribution comes from 1^+ and 2^+ final states, almost half coming from the 2^+ state at ≈3.6 MeV in ^{12}N. Überall and co-workers [12] do not specifically quote cross sections for muon-decay neutrino spectra, but find total cross sections to excited states in agreement with Ref. [7], although there are disagreements with regard to specific final states. Donnelly [7] gives a prediction for the ratio of (exclusive)/(inclusive) cross sections, $\mathcal{R}=0.72$.

There is generally good agreement between calculation and the measured values of cross sections and of the ratio of cross sections. The present experimental precision ($\pm15\%$) must be improved to make a significant test of the theoretical calculations of ν_e ^{12}C reactions.

C. Inclusive ^{13}C(ν_e,e^-)X cross section

There was no unambiguous signal for neutrino reactions with any nucleus except ^{12}C. An upper limit on the weighted sum of cross sections for $\nu_e(^{13}\mathrm{C}+^{27}\mathrm{Al})$ was presented in Eq. (5); this limit corresponds to a 90% bound of $\langle\sigma\rangle<10.6\times10^{-41}$ cm^2 on the mean neutrino-absorption cross section. The neutrino-absorption cross section for these two nuclei are expected to be roughly equal, but complete calculations of inclusive reactions only exist for the ^{13}C target.

One group [14] has published estimates for muon-decay neutrino-induced transitions to explicit final states in ^{13}N; 2.2×10^{-41} cm^2 for transitions to the ^{13}N ground state and 2.3×10^{-41} cm^2 to the 3.65 MeV $(\frac{3}{2})^-$ excited state. These values supersede previous results [13] which did not constrain the form factors according to measured analog transition rates. However, the greatest difference between the earlier and later calculation was a factor of 3 reduction in the cross section to the 3.65 MeV excited state, and a 50% reduction in the inclusive (all final-state) event rate to reflect possible Gamow-Teller quenching of the nuclear matrix element. On the other hand, the inclusive cross section obtained from Ref. [13] is in agreement with an unpublished result from Donnelly [21]; neglecting the possible Gamow-Teller quenching effect, but including form-factor constraints imposed by beta-decay and analog transition rates, the exclusive cross sections for the ^{13}N(g.s.) and 3.65 MeV final states published in Ref. [13] are also in very good agreement with Ref. [21].

While the upper limit reported here cannot be taken as evidence for, or against, quenching of the nuclear matrix element, the analysis does encourage future explorations. The ν_e ^{13}C electron distribution is easily distinguished from the "irreducible" backgrounds from νe^- elastic scattering and ν_e ^{12}C inverse-beta decay, as evidenced by the stability of the fit results for those components. However, in this experiment, the ν_e ^{13}C signal was unresolved from residual neutron-induced backgrounds; those backgrounds could be practically eliminated by more complete shielding.

VII. CONCLUSIONS

We have obtained the first measurement of a neutrino-induced reaction between specific nuclear states. The cross section for ^{12}C(ν_e,e^-)^{12}N(g.s.), $(1.05\pm0.14)\times10^{-41}$ cm^2, is in agreement with the theoretical estimates. The energy and angular dependence of the measured signal is consistent with expectations. A measurement of inclusive neutrino-nuclear reactions results in a total cross section of $(1.41\pm0.23)\times10^{-41}$ cm^2 for ν_e ^{12}C absorption. The ratio of exclusive-to-inclusive cross sections, which may provide a test of the nuclear physics approximations made in the theoretical calculations, is $\mathcal{R}=0.74\pm0.14$. There is only weak evidence for the observation of neutrino-nuclear reactions with other nuclei; upper limits consistent with present theoretical calculations are obtained.

These measurements demonstrate the feasibility of observing low-energy neutrino-induced transitions between specific nuclear states. The possibility exists to use certain exclusive transitions as "spin-isospin" filters [11] to provide new types of investigations of nuclear physics or searches for exotic weak nuclear currents outside of the standard model. Other future investigations may include direct calibration of cross sections of astrophysical interest or novel searches for neutrino oscillations.

ACKNOWLEDGMENTS

We would like to express particular thanks to N. Briscoe, C. Dalton, R. S. DeLay, H. Juds, G. Krausse, A. J. Sena, and T. N. Thompson for building, operating, and maintaining the detector with extreme professionsalism. Dr. V. Bharadwaj, Dr. G. Brooks, Dr. M. Duong-Van, and Dr. A. M. Rushton contributed to early phases of this experiment, and R. Bartolo and Dr. H. Yao assisted in the Monte Carlo simulation of the neutrino-absorption signals. We thank Prof. T. W. Donnelly for programs to calculate neutrino-absorption cross sections and for helpful discussions. This work was supported by the U.S. Department of Energy, Nuclear Physics Division and High Energy Physics Division, under Contract Nos. W-31-109-ENG-38, DE-AC05-76-ERO-2504, and W-7405-ENG-36 and by the U. S. National Science Foundation, Grant No. PHY85-01559.

[1] R. W. Manweiler, *et al.*, in *Intersections Between Particle and Nuclear Physics,* Proceedings of a Conference held in Rockport, Maine, 1988, AIP Conference Proceedings No. 176, edited by G. Bunce (AIP, New York, 1988), p. 912.
[2] S. Willis, Ph.D. thesis, 1979 (Los Alamos Scientific Laboratory Report LA-8030-T); S. Willis *et al.,* Phys. Rev. Lett. **44**, 522 (1980).
[3] F. Reines, H. W. Sobel, and E. Pasierb, Phys. Rev. Lett. **45**, 1307 (1980).
[4] J. N. Bahcall and R. K. Ulrich, Rev. Mod. Phys. **60**, 297 (1988).
[5] R. C. Allen *et al.,* Phys. Rev. Lett. **64**, 1871 (1990).
[6] B. Bodmann *et al.*, Karmen Collaboration, Phys. Lett. B **267**, 321 (1991).
[7] T. W. Donnelly, Phys. Lett. **43B**, 93 (1973).
[8] S. L. Mintz and M. Pourkaviani, Phys. Rev. C **40**, 2458 (1989).
[9] M. Fukugita, Y. Kohyama, and K. Kubodera, Phys. Lett. B **212**, 139 (1988).
[10] J. S. O'Connell, T. W. Donnelly, and J. D. Walecka, Phys. Rev. C **6**, 719 (1972).
[11] T. W. Donnelly and R. E. Peccei, Phys. Rep. **50**, 1 (1979).
[12] Francis J. Kelly and H. Überall, Phys. Rev. C **5**, 1432 (1972); H. Überall, Bernhard A. Lamers, James B. Langworthy, and Francis J. Kelly, *ibid.* **6**, 1911 (1972).
[13] J. Arafune, M. Fukugita, Y. Kohyama, and K. Kubodera, Phys. Lett. B **217**, 186 (1989).
[14] M. Fukugita, Y. Kohyama, K. Kubodera, and T. Kuramoto, Phys. Rev. C **41**, 1359 (1990).
[15] R. L. Burman, M. E. Potter, and E. S. Smith, Nucl. Instrum. Methods Phys. Res., Sect. A **291**, 621 (1990).
[16] R. C. Allen, H. H. Chen, M. E. Potter, R. L. Burman, J. B. Donahue, V. D. Sandberg, D. A. Krakauer, R. L. Talaga, E. S. Smith, and A. C. Dodd, Nucl. Instrum. Methods Phys. Res., Sect. A **284**, 347 (1989).
[17] R. C. Allen *et al.,* Nucl. Instrum. Methods Phys. Res. Sect. A **269**, 177 (1988).
[18] D. A. Krakauer, Ph.D. thesis, University of Maryland, 1989; Los Alamos National Laboratory Report LA-12262-T, 1992.
[19] D. A. Krakauer *et al.,* Phys. Lett. B **263**, 534 (1991).
[20] R. C. Allen *et al.,* Los Alamos National Laboratory Report LA-11300-P, 1988.
[21] T. W. Donnelly (private communication).
[22] R. C. Allen *et al.,* Phys. Rev. Lett. **64**, 1330 (1990).